AIMS Bioengineering

AIMS Bioengineering, 11(2): 266–280.
DOI: 10.3934/bioeng.2024014
Received: 20 April 2024
Revised: 20 April 2024
Accepted: 26 June 2024
Published: 17 July 2024

http://www.aimspress.com/journal/Bioengineering

Research article

Integration of bifurcation analysis and optimal control of a molecular network

Lakshmi N Sridhar*

Department of Chemical Engineering, University of Puerto Rico, Mayaguez PR 00681

*** Correspondence:** Email: lakshmin.sridhar@upr.edu.

Abstract: Molecular biological networks are highly nonlinear systems that exhibit limit point singularities. Bifurcation analysis and multiobjective nonlinear model predictive control (MNLMPC) of a molecular network problem represented by the Pettigrew model were performed. The Matlab program MATCONT (Matlab continuation) was used for the bifurcation analysis and the optimization language PYOMO (python optimization modeling objects) was used for performing the multiobjective nonlinear model predictive control. MATCONT identified the limit points, branch points, and Hopf bifurcation points using appropriate test functions. The multiobjective nonlinear model predictive control was performed by first performing single objective optimal control calculations and then minimizing the distance from the Utopia point, which was the coordinate of minimized values of each objective function. The presence of limit points (albeit in an infeasible region) enabled the MNLMPC calculations to result in the Utopia solution. MNLMPC of the partial models also resulted in Utopia solutions.

Keywords: molecular network; optimal control; bifurcation; Utopia solution

1. Introduction

Molecular biological networks are complex systems with a high degree of nonlinearity [1–4]. The presence of singularities in the form of limit points in the Pettigrew model for molecular networks was demonstrated by Song and co-workers [5], Sridhar [6] showed for small-scale problems that the presence of singularities in the form of limit and branch points are beneficial for multiobjective nonlinear model predictive calculations and enable one to obtain the best possible solution (Utopia Point). The aim of this paper is to demonstrate that in the molecular network problem where the

Pettigrew model is used, the presence of limit points (albeit in an infeasible region) can benefit the multiobjective nonlinear model predictive calculations, and the result obtained is the Utopia solution. This paper is organized as follows. First, the background section dealing with the work done on molecular network models is described. This is followed by a description of the bifurcation analysis techniques and the strategy for performing the multiobjective nonlinear model predictive control calculations. A section on the interaction between bifurcation analysis and multiobjective nonlinear model predictive control is followed by a description of the Pettigrew model. The results and discussion section are then presented followed by the conclusions.

2. Background

Several workers did a considerable amount of work on biological networks. Pinsker et al. [7] looked at long-term sensitization of a defensive withdrawal reflex in Aplysia California. Frost et al. [8] studied monosynaptic connections made by the sensory neurons of the gill- and siphon-withdrawal reflex in Aplysia participate in the storage of long-term memory for sensitization. Scholz and Byrne, 1987 investigated long-term sensitization in Aplysia: Biophysical correlates in tail sensory neurons. Walters and co-workers [9,10] developed a simple model of long-term hyperalgesia and multiple sensory neuronal correlates of site-specific sensitization in Aplysia.

Castellucci et al. [11] 1989 showed that inhibition of protein synthesis blocks long-term behavioral sensitization in the isolated gill-withdrawal reflex of Aplysia. Goldsmith and Byrne [2] discovered that bag cell extract inhibits tail-siphon withdrawal reflex, suppresses long-term but not short-term sensitization, and attenuates sensory-to-motor neuron synapses in Aplysia. Cleary [12] further studied cellular correlates of long-term sensitization in Aplysia. Wright et al. [13] 1scussed the developmental emergence of long-term memory for sensitization in Aplysia. Levenson et al. [14] showed that serotonin levels in the hemolymph of Aplysia are modulated by light/dark cycles and sensitization training. Sutton et al. [15] studied the interaction between the amount and pattern of training in the induction of intermediate and long-term memory for sensitization in Aplysia. Wainwright et al. [16] investigated localized neuronal outgrowth induced by long-term sensitization training in Aplysia. Wainwright et al. [17] studied the dissociation of morphological and physiological changes associated with long-term memory in Aplysia.

Pettigrew and co-workers [18] developed a model that represents short (STF)-, intermediate (ITF)-, and long (LTF)-term phases of protein kinase A (PKA) activation and corresponding phases of facilitation of the Aplysia sensorimotor synapse. This model studies biophysical mechanisms that may be implicated in learning and memory. The model also represents phosphorylation of the transcription factor CREB1 (cyclic adenosine monophosphate responsive element binding protein 1) by PKA and induction of the immediate-early gene Aplysia ubiquitin hydrolase (Ap-uch); Ap-uch is necessary for LTF. PKA and ERK (Extra-cellular Signal Regulated Kinase) activation, CREB1 and CREB2 phosphorylation, and Ap-uch induction are dealt with in this model where biochemical processes in the presynaptic sensory neuron that contribute to STF, ITF, and LTF of the sensorimotor synapse are represented. More details of this model can be found in Pettigrew et al. [18] and Song et al. [19]. Song et al. [19] demonstrates the existence of limit points that cause multiple steady-states for unrealistic parameters of the Pettigrew model. The aim of this paper is to show that the limit points (even if found in the infeasible region) are beneficial in obtaining the Utopia solution when multiobjective nonlinear model predictive calculations are performed.

3. Bifurcation analysis

There has been a lot of work in chemical engineering involving bifurcation analysis throughout the years. The existence of multiple steady-states and oscillatory behavior in chemical processes has led to a lot of computational and analytical work to explain the causes for these nonlinear phenomena. Multiple steady states are caused by the existence of branch and limit points while oscillatory behavior is caused by the existence of Hopf bifurcations points.

In the case of branch points and limit points, the Jacobian matrix of the set of steady-state equations is singular. However, at a branch point, there are 2 distinct tangents at the singular point, while at a limit point, there is only one tangent at the singular point. Singularities in the Jacobian matrix is often indicative of an optimal solution and this motivates the investigation of how the singular points in the Jacobian matrix, indicated by branch and limit points, would affect the multiobjective dynamic optimization.

One of the most commonly used software to locate limit points, branch points, and Hopf bifurcation points is MATCONT (Dhooge et al, [20,21]). This software detects limit points, branch points, and Hopf bifurcation points. Consider an ODE (ordinary differential equation) system

$$\dot{x} = f(x, \beta) \tag{1}$$

where $x \in R^n$. Let the tangent plane at any point x be $[v_1, v_2, v_3, v_4, ...v_{n+1}]$. Define matrix A given by

$$A = \begin{bmatrix} \frac{\partial f_1}{\partial x_1} & \frac{\partial f_1}{\partial x_2} & \frac{\partial f_1}{\partial x_3} & \frac{\partial f_1}{\partial x_4} \cdots\cdots\cdots \frac{\partial f_1}{\partial x_n} & \frac{\partial f_1}{\partial \beta} \\ \frac{\partial f_2}{\partial x_1} & \frac{\partial f_2}{\partial x_2} & \frac{\partial f_2}{\partial x_3} & \frac{\partial f_2}{\partial x_4} \cdots\cdots\cdots \frac{\partial f_2}{\partial x_n} & \frac{\partial f_2}{\partial \beta} \\ \cdots\cdots\cdots\cdots\cdots\cdots\cdots\cdots\cdots\cdots\cdots\cdots\cdots\cdots\cdots\cdots\cdots\cdots\cdots\cdots\cdots\cdots \\ \cdots\cdots\cdots\cdots\cdots\cdots\cdots\cdots\cdots\cdots\cdots\cdots\cdots\cdots\cdots\cdots\cdots\cdots\cdots\cdots\cdots\cdots \\ \frac{\partial f_n}{\partial x_1} & \frac{\partial f_n}{\partial x_2} & \frac{\partial f_n}{\partial x_3} & \frac{\partial f_n}{\partial x_4} \cdots\cdots\cdots \frac{\partial f_n}{\partial x_n} & \frac{\partial f_n}{\partial \beta} \end{bmatrix} \tag{2}$$

The matrix A can be written in a compact form as

$$A = [B| \quad \frac{\partial f}{\partial \beta}] \tag{3}$$

The tangent surface must satisfy the equation

$$Av = 0 \tag{4}$$

For both limit and branch points, the matrix B must be singular. For a limit point, the n+1th component of the tangent vector v_{n+1} = 0 and for a branch point the matrix $\begin{bmatrix} A \\ v^T \end{bmatrix}$ must be singular. For a Hopf bifurcation, the function should be zero. e indicates the bialternate product while I_n is the n-square identity matrix. More details can be found in Kuznetsov [22,23] and Govaerts [24].

3.1. The multiobjective nonlinear model predictive control (MNLMPC) method

The MNLMPC method was first proposed by Flores Tlacuahuaz et al. [25] and used by Sridhar [26–30]. Similar optimization work was done by Younius and co-workers [31–33] and Safari [34]. This method is rigorous and it does not involve the use of weighting functions nor does it impose additional parameters or additional constraints on the problem unlike the weighted function or the epsilon correction method (Miettinen [35]). For a problem that is posed as

$$\begin{aligned} & min\, J\,(x,u) = (x_1, x_2 \ldots . x_k) \\ subject\ to\ \ & \frac{dx}{dt} = F(x,u); h(x,u) \le 0; x^L \le x \le x^U; u^L \le u \le u^U \end{aligned} \tag{5}$$

The MNLMPC method first solves dynamic optimization problems independently, minimizing/maximizing each x_i individually. The minimization/maximization of x_i will lead to x_i^*. Then, the optimization problem that will be solved is

$$\begin{aligned} & min \sqrt{\{x_i - x_i^*\}^2} \\ subject\ to\ \ & \frac{dx}{dt} = F(x,u); h(x,u) \le 0; x^L \le x \le x^U; u^L \le u \le u^U \end{aligned} \tag{6}$$

3.1.1. The MOOC calculation

It will provide the control values for various times. The first obtained control value is implemented and the remaining are discarded. This procedure is repeated until the implemented and the first obtained control value are the same. The optimization package in Python, Pyomo, Hart, et al. [36], is commonly used and is where the differential equations are automatically converted to a nonlinear program (Biegler [37]. The state-of-the-art solvers like IPOPT (interior point optimizer), Wachter and Biegler [38] and BARON (branch-and-reduce optimization navigator), Tawaralmani and Sahinidis [39] are normally used in conjunction with PYOMO (python optimization modeling objects)).

The steps of the algorithm are as follows:

1. Minimize/maximize x_i subject to the differential and algebraic equations that govern the process using PYOMO and Baron. This will lead to x_i^*.

2. Minimize $\sqrt{\{x_i - x_i^*\}^2}$ (multiobjective function) subject to the differential and algebraic equations that govern the process. This is the MOOC calculation and provides the control values for various times. If this calculation obtains a value of zero for the multiobjective function, then the Utopia point is obtained and the calculations are terminated. Otherwise, we proceed to step 3.

3. Implement the first obtained control values and discard the remaining.

4. Repeat steps 1 to 3 until there is an insignificant difference between the implemented and the first obtained value of the control variables.

3.2. Effect of singularities (limit point and branch point) on MNLMPC

Let the minimization be of the variable p_1 lead to the value M_1 and the minimization of function p_2 lead to the value M_2. This is equivalent to minimizing $(p_1 - M_1)^2$ and $(p_2 - M_2)^2$. The subsequent multiobjective minimization will be of the function $(p_1 - M_1)^2 + (p_2 - M_2)^2$.

The multiobjective optimal control problem is

$$\begin{gathered} min \; (p_1 - M_1)^2 + (p_2 - M_2)^2 \\ subject\ to \quad \frac{dx}{dt} = F(x,u) \end{gathered} \tag{7}$$

For all i,

$$\frac{d}{dx_i}((p_1 - M_1)^2 + (p_2 - M_2)^2) = 2(p_1 - M_1)\frac{d}{dx_i}(p_1 - M_1) + 2(p_2 - M_2)\frac{d}{dx_i}(p_2 - M_2) \tag{8}$$

At the Utopia point both $(p_1 - M_1)$ and $(p_2 - M_2)$ are zero. Hence,

$$\frac{d}{dx_i}((p_1 - M_1)^2 + (p_2 - M_2)^2) = 0 \tag{9}$$

Now let us look at the co-state equation

$$\begin{gathered} \frac{d}{dt}(\lambda_i) = -\frac{d}{dx_i}((p_1 - M_1)^2 + (p_2 - M_2)^2) - g_x\lambda_i \\ \lambda_i(t_f) = 0 \end{gathered} \tag{10}$$

The first term in this equation is 0 and hence

$$\begin{gathered} \frac{d}{dt}(\lambda_i) = -g_x\lambda_i \\ \lambda_i(t_f) = 0 \end{gathered} \tag{11}$$

If the set of ODE $\frac{dx}{dt} = g(x,u)$ has a limit or a branch point, g_x is singular.

Hence there are two different vectors-values for $[\lambda_i]$ where $\frac{d}{dt}(\lambda_i) > 0$ and $\frac{d}{dt}(\lambda_i) < 0$. In between there is a vector $[\lambda_i]$ where $\frac{d}{dt}(\lambda_i) = 0$. This coupled with the boundary condition $\lambda_i(t_f) = 0$ will lead to $[\lambda_i] = 0$ (The subscript f stands for final which will make the problem an unconstrained optimization problem and the one and only solution for the unconstrained problem is the Utopia solution).

3.2.1. Pettigrew model

The variables in this model are the following:
(1) PKA
(2) Ap-uch
(3) cAMP

(4) C (Catalytic subunit)
(5) R (Regulatory subunit)
(6) RC PKA (holoenzyme)
(7) REG (hypothetical protein)
(8) PREG (phosphorylated REG)
(9) $mRNA_{REG}$ REG mRNA (proteins)
(10) RAF, MAPKK, ERK (proteins)
(11) MAPKK (mitogen-activated protein kinases kinases)
(12) ERK (extracellular signal-regulated kinases)
(13) MAPKKp (phosphorylated MAPPK)
(14) MAKKpp (phosphorylated MAPPKp)
(15) ERKp (phosphorylated ERK)
(16) P_{ERK} (fraction of CREB2 sites phosphorylated by ERK)
(17) P_{PKA} (fraction of available CREB1 sites phosphorylated by PKA)

The model parameter values are

V_{syn} = 0.002, K_{fpka} = 105, $K_{kp\text{-}uch}$ = 0.007, AP-uch_{basal} = 0.1, K_{fdka} = 0.00048,τ = 250, K_{baskpa} = 12, K_{reg} = 0.00064, $K_{translation}$ = 4, ν_{rphos} = 1, K_{rhos} = 1.5, V_{dreg} = 0.16, K_{dreg} = 0.0015, ,K_{dsm} = 0.02, V_{mreg} = 0.00002, $K_{b,\ raf}$ = 0.001, $K_{b,\ mapkk}$ = 0.12, $K_{b,\ erk}$ = 0.12, Raf_{tot} = 0.5, $MAPKK_{tot}$ = 0.5, ERK_{tot} = 0.5, K_{MK} = 0.08, ERK_{basal} = 0.0015, K_{phos1} = 0.1, $K_{dephos1}$ = 1.5, PPhos = 0.1, K_{phos2} = 0.005, $K_{dephos2}$ = 0.5, K_{apsyn} = 0.02, $K_{apsynbasal}$ = 0.0009, K_{pka} = 0.2, K_{erk} = 0.004, K_{deg} = 0.01.

The model equations are

$$\frac{d[cAMP]}{dt} = 3.6 * [\frac{5 - HT}{5 - HT + 14}] - cAMP - 0.06! \text{ [unknown template]} \tag{12}$$

$$\frac{dR}{dt} = V_{syn} + k_{fpka}[RC][cAMP]^2 - k_{bpka}[R][C] - k_{Ap-Uch}R([Ap - Uch] - [Ap - Uch_{basal}]) - k_{dpka}R \tag{13}$$

$$\frac{dC}{dt} = V_{syn} + k_{fpka}[RC][cAMP]^2 - k_{bpka}[R][C] + k_{Ap-Uch}[RC]([Ap - Uch] - [Ap - Uch_{basal}]) - k_{dpka}C \tag{14}$$

$$\frac{d[RC]}{dt} = -k_{fpka}[RC][cAMP]^2 + k_{bpka}[R][C] - k_{Ap-Uch}[RC]([Ap - Uch] - [Ap - Uch_{basal}]) - k_{dpka}[RC] \tag{15}$$

$$[PKA]_{act} = [C] \quad k_{bpka} = (\frac{k_{baspka}}{1 + \frac{pREG}{k_{reg}}}) \tag{16}$$

$$\frac{d[REG]}{dt} = k_{translation}[mRNA_{REG}][ERK_{act}] - \nu_{dreg}(\frac{pREG}{REG + K_{dreg}}) - k_{dsm}[REG] \tag{17}$$

$$\frac{d[pREG]}{dt} = v_{rphos} ERK_{act} \left(\frac{REG - pREG}{REG - pREG + K_{rphos}}\right) - v_{dreg} \left(\frac{pREG}{REG + K_{dreg}}\right) - k_{dsm}[pREG] \quad (18)$$

$$\frac{d[mRNA_{reg}]}{dt} = v_{mREG} - v_{dmREG}[5 - HT] + \frac{mRNA_{REG}}{mRNA_{REG} + K_{dmreg}} - (mRNA_{REG} K_{dmreg}) \quad (19)$$

$$\frac{d[Raf]}{dt} = -k_{f-raf}[5 - HT][Raf] + k_{b-raf}[5 - HT][Raf_{tot} - Raf] \quad (20)$$

$$\frac{d(MAPKK)}{dt} = -k_{f,Raf}[Raf_{tot} - Raf]\left[\frac{MAPKK}{MAPKK + K_{MR}}\right] + k_{b,MAPKK}\left[\frac{MAPKK^{p}}{MAPKK^{p} + K_{MK}}\right] \quad (21)$$

$$\frac{d(MAPKK^{PP})}{dt} = -k_{f,MAPKK}[Raf_{tot} - Raf]\left[\frac{MAPKK^{p}}{MAPKK^{p} + K_{MR}}\right] - k_{b,MAPKK}\left[\frac{MAPKK^{pp}}{MAPKK^{pp} + K_{MK}}\right] \quad (22)$$

$$\frac{d(P_{ERK})}{dt} = k_{phos,2} ERK_{act}(1 - P_{ERK}) - k_{dephos,2} PhosP_{ERK} \quad (23)$$

$$\frac{d(Ap - Uch)}{dt} = k_{ApSyn} MAPPK^{pp}\left(\frac{P_{pka}^{2}}{P_{pka}^{2} + K_{pka}^{2}}\right)\left(\frac{P_{erk}^{2}}{P_{erk}^{2} + K_{erk}^{2}}\right) + k_{ApSynbasal} - k_{deg} \quad (24)$$

4. Results and discussion

4.1. Full model bifurcation analysis and MNLMPC

4.1.1. Bifurcation analysis

The bifurcation analysis was performed using MATCONT and reveals the presence of 2 limit points as shown in Figure 1. Although these limit points are in an infeasible region with 5-HT having negative values, their presence results in the Utopia solution when the MNLMPC calculations are performed.

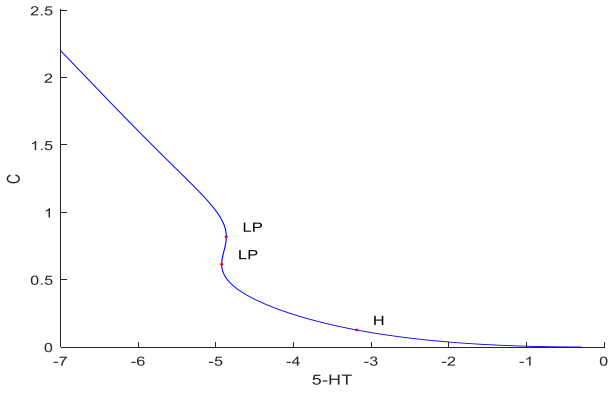

Figure 1. Bifurcation diagram indicating limit points.

4.1.2. MNLMPC

The full model represented by Eqs 12–24 were considered and C, MAPKK, RAF, ERK, REG and PREG are clubbed together as $\sum C_i + REG_i + PREG_i + RAF_i + ERK_i + +MAPKK_i$. The maximization of this objective function yields a value of 41.918 and the minimization of $\sum R_i$ results in a value of 0. The MNLMPC calculations were performed by minimizing $\sum C_i + REG_i + PREG_i + RAF_i + ERK_i + MAPKK_i$ and resulted in the utopia solution with the objective function value being 0 and the obtained control value of 5-HT of 1.242. The profiles are represented in Figures 2 and 3.

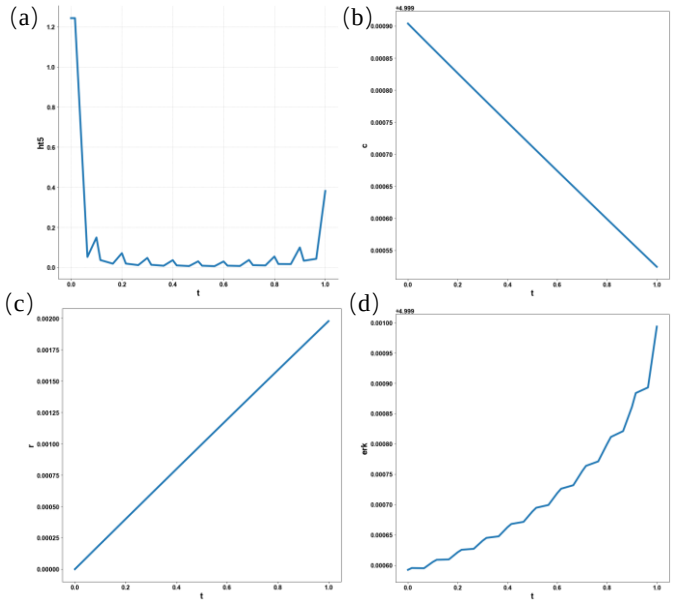

Figure 2. (a) Full Model MNLMPC ht5 vs t; (b) Full Model MNLMPC c vs t; (c) Full Model MNLMPC r vs t; (d) Full Model MNLMPC erk vs t.

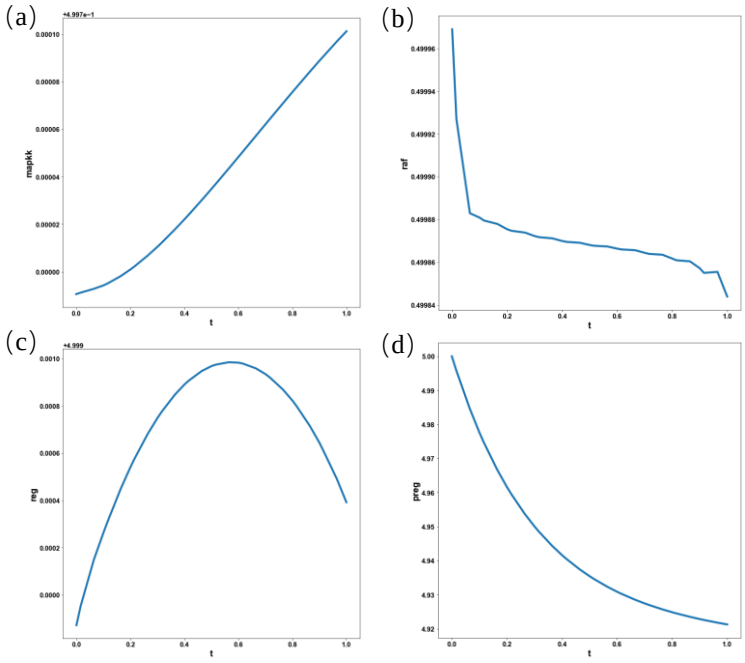

Figure 3. (a) Full Model MNLMPC mapkk vs t; (b) Full Model MNLMPC raf vs t; (c) Full Model MNLMPC reg vs t; (d) Full Model MNLMPC preg vs t.

4.1.3. MNLMPC for model PKA activity after exposure to 5-HT and hydrolysis of PKA R-subunits by Ap-uch

The Eqs 12–16 are considered. Here, $\sum C_i$ is maximized and yields a value of 10 and $\sum R_i$ is minimized to yield a value of 0. The MNLMPC calculations were performed by minimizing $(\sum C_i - 10)^2 + (\sum R_i - 0)^2$ and yields the Utopia point with the objective function value of 0. Unfortunately, the 5-HT profiles exhibited spiked behavior (Figure 4a). This was remedied using a tanh activation factor $\frac{(5-HT)\tanh(5-HT)}{\varepsilon}$, and the spikes were considerably controlled (Figure 4b). Even with this correction, the utopia point was obtained and with the objective function value of 0. The C vs t profiles are shown in Figure 4c,d. The MNLMPC control value obtained was 0.73. All values are positive and there is no upper limit for the variables.

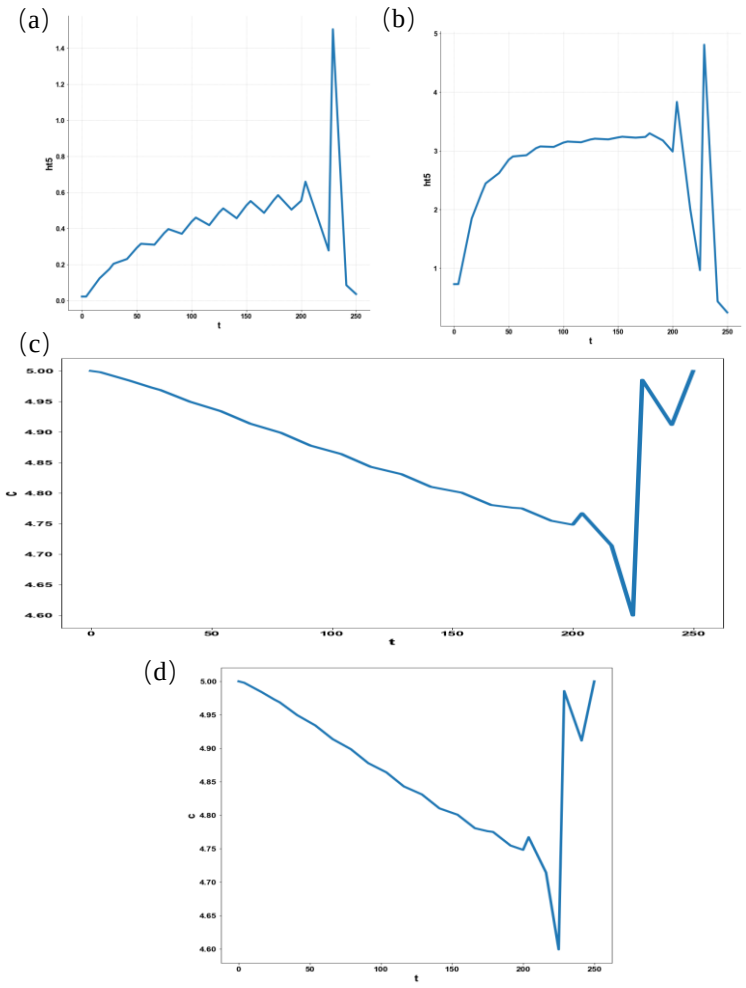

Figure 4. (a) Pka activity model MNLMPC ht5 vs t without taanh activation factor; (b) Pka activity model MNLMPC ht5 vs t with tanh activation factor; (c) Pka activity model MNLMPC c vs t without activation factor; (d) Pka activity model MNLMPC c vs t wit activation factor.

4.1.4. MNLMPC for modeling REG and PREG dynamics

The Eqs 17–19 are considered. Both $\sum REG_i$ and $\sum PREG_i$ are maximized yielding values of 10 and 9.92 The MLMNPC calculations were performed minimizing $(\sum REG_i - 10)^2 + (\sum PREG_i - 9.92)^2$. Unfortunately, the 5-HT profiles exhibited spiked behavior (Figure 5a). This was remedied using the tanh activation factor $\frac{(5-HT)\tanh(5-HT)}{\varepsilon}$ and the spikes were considerably controlled (Figure 5b). The MLMNPC calculations yields the Utopia point with the objective function value of 0 and the MNLMPC control value of 5-HT was 2.86. The REG vs t and the PREG vs t profiles are shown in Figure 5c,d.

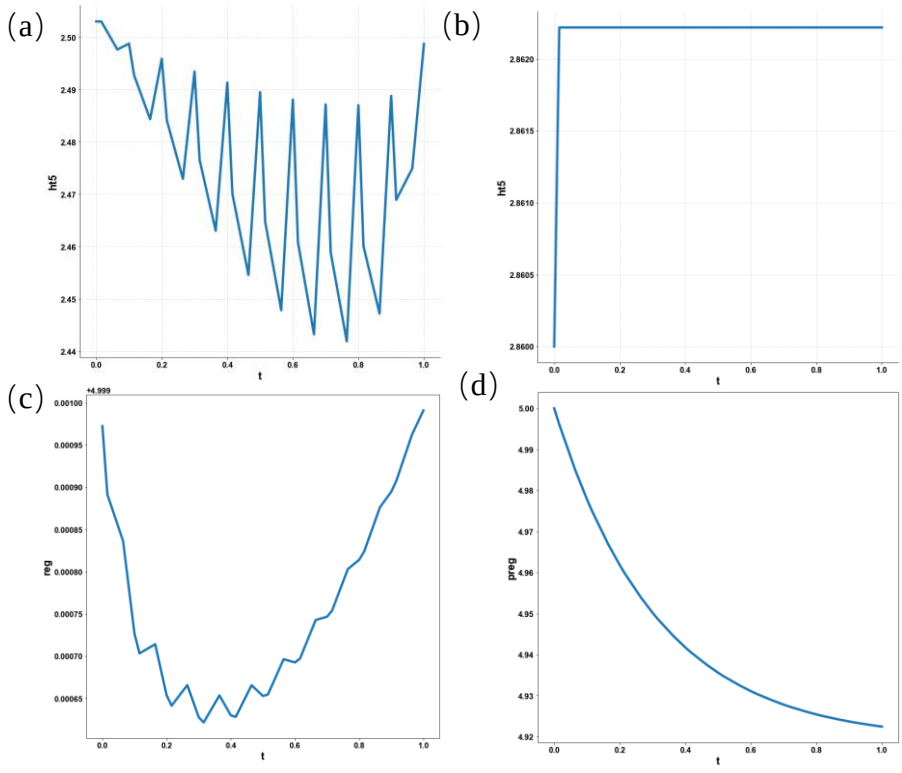

Figure 5. (a) MNLMPC for modelling ht5 vs t without activation factor; (b) MNLMPC for modelling ht5 vs t with activation factor; (c) MNLMPC for modelling REG dynamics reg vs t with activation factor; (d) MNLMPC for modelling PREG dynamics with activation factor.

4.1.5. MNLMPC for modeling the Raf/MEK/ERK pathway

Eqs 22–24 are considered. $\sum MAPKK_i, \sum ERK_i$ and $\sum RAF_i$, are maximized to yield values of 1, 1 and 10 respectively. The MLMNPC calculations were performed minimizing $(\sum MAPKK_i - 1)^2 + (\sum ERK_i - 10)^2 + (\sum RAF_i - 1)^2$. Unfortunately, the 5-HT profiles exhibited spiked behavior (Figure 6a). This was remedied using a tanh activation factor $\frac{(5-HT)\tanh(5-HT)}{\varepsilon}$ and the spikes were considerably controlled (Figure 6b). This yielded the Utopia point with the objective function value of 0, and the MNLMPC control value of 5-HT was 3.206. Figure 6c–e shows the ERK, MAPKK, and RAF profiles.

The full model exhibits limit points and the presence of the limit points guarantees that the Utopia solution would be obtained in a MNLMPC calculation. Similar to the MNLMPC calculations for the full model that results in the Utopia point, the MNLMPC calculations for the partial models also result in the Utopia point. A comparison of Figures 2c and 3c show that the MNLMPC of the full model is better than that of the partial model as the value of C (PKA_{act}) is higher when the MNLMPC of the full model is performed. The lower limit for these values is 0.

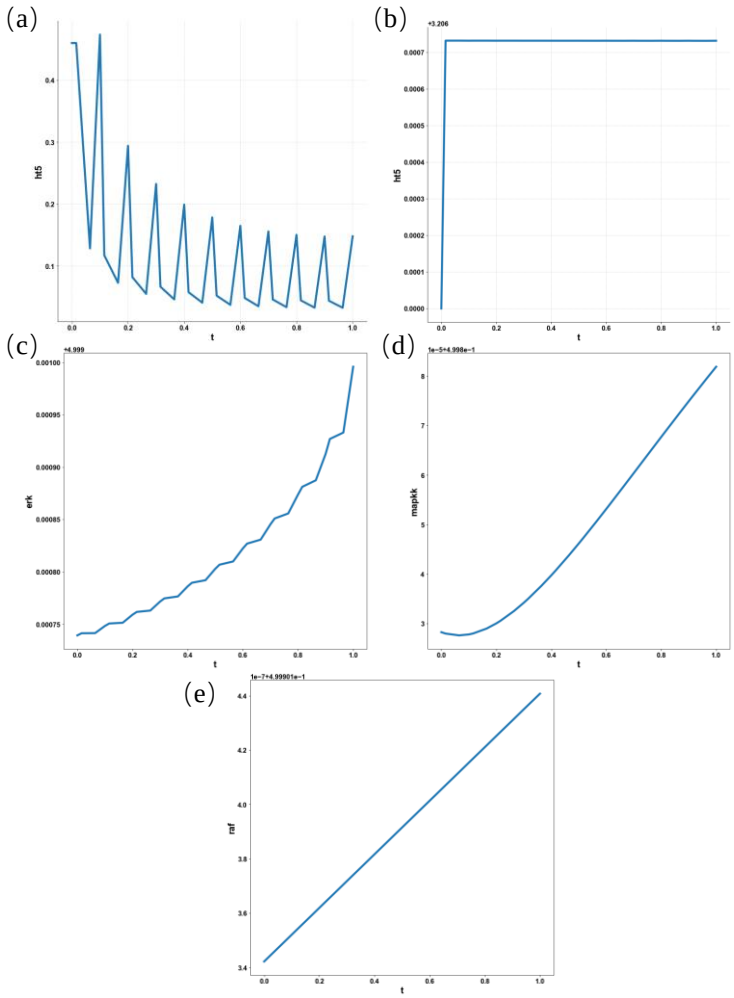

Figure 6. (a) MNLMPC for modelling the Raf/MEK/ERK pathway ht5 vs t no activation factor used; (b) MNLMPC for modelling the Raf/MEK/ERK pathway ht5 vs t with activation factor used; (c) MNLMPC for modelling the Raf/MEK/ERK pathway erk vs t; (d) MNLMPC for modelling the Raf/MEK/ERK pathway mapKK vs t; (e) MNLMPC for modelling the Raf/MEK/ERK pathway raf vs t.

5. Conclusions

Bifurcation analysis and nonlinear model predictive control was performed for the Pettigrew model. The bifurcation analysis revealed the existence of limit points (albeit in the infeasible region). The MNLMPC calculations (for both the partial and full models) resulted in the Utopia solution. An integration of the bifurcation analysis and MNLMPC revealed that the existence of the limit points was beneficial and enabled the MNLMPC calculations to result in the Utopia solution.

Use of AI tools declaration

The authors declare they have not used Artificial Intelligence (AI) tools in the creation of this article.

Data availability statement

All data used is presented in the paper.

Conflict of interest

The author, Dr. Lakshmi N Sridhar has no conflict of interest.

References

1. Smolen P, Baxter DA, Byrne JH (2000) Mathematical modelling of gene networks. *Neuron* 26: 567–580. https://doi.org/10.1016/S0896-6273(00)81194-0
2. Goldsmith JR, Byrne JH (1993) Bag cell extract inhibits tail-siphon withdrawal reflex, suppresses long-term but not short-term sensitization, and attenuates sensory-to-motor neuron synapses in Aplysia. *J Neurosci* 13: 1688–1700. https://doi.org/10.1523/JNEUROSCI.13-04-01688.1993
3. Goldbeter A (2002) Computational approaches to cellular rhythms. *Nature* 420: 238–245. https://doi.org/10.1038/nature01259
4. Kitano H (2002) Systems biology: A brief overview. *Science* 295: 1662–1664. https://doi.org/10.1126/science.1069492
5. Song H, Smolen P, Av-Ron E, et al. (2006) Bifurcation and singularity analysis of a molecular network for the induction of long-term memory. *Biophys J* 90: 2309–2325. https://doi.org/10.1529/biophysj.105.074500
6. Sridhar LN (2023) Multi objective nonlinear model predictive control of diabetes models considering the effects of insulin and exercise. *Archives Clin Med Microbiol* 2: 60–69. https://doi.org/10.33140/ACMMJ
7. Pinsker H, Carew TJ, Hening W, et al. (1973) Long-term sensitization of a defensive withdrawal reflex in Aplysia californica. *Science* 182: 1039–1042. https://doi.org/10.1126/science.182.4116.1039
8. Frost WN, Castelluci VF, Hawkins RD, et al. (1985) Monosynaptic connections made by the sensory neurons of the gill and siphon-withdrawal reflex in Aplysia participate in the storage of long-term memory for sensitization. *Proc Natl Acad Sci* 82: 8266–8269. https://doi.org/10.1073/pnas.82.23.8266
9. Walters ET (1987) Site-specific sensitization of defensive reflexes in Aplysia: A simple model of long-term hyperalgesia. *J Neurosci* 7: 400–407. https://doi.org/10.1523/jneurosci.07-02-00400.1987
10. Walters ET (1987) Multiple sensory neuronal correlates of site-specific sensitization in Aplysia. *J Neurosci* 7: 408–417. https://doi.org/10.1523/jneurosci.07-02-00400.1987
11. Castellucci VF, Blumenfeld H, Goelet P, et al. (1989) Inhibitor of protein synthesis blocks long-term behavioral sensitization in the isolated gill-withdrawal reflex of Aplysia. *J Neurobiol* 20: 1–9. https://doi.org/10.1002/neu.480200102
12. Cleary LJ, Lee WL, Byrne JH (1998) Cellular correlates of long-term sensitization in Aplysia. *J Neurosci* 18: 5988–5998. https://doi.org/10.1101/lm.045450.117

13. Wright WG, McCance EF, Carew TJ (1996) Developmental emergence of long-term memory for sensitization in Aplysia. *Neurobiol Learn Mem* 65: 261–268. https://doi.org/10.1006/Nlme.1996.0031
14. Levenson J, Byrne JH, Eskin A (1999) Levels of serotonin in the hemolymph of Aplysia are modulated by light/dark cycles and sensitization training. *J Neurosci* 19: 8094–8103. https://doi.org/10.1523/JNEUROSCI.19-18-08094.1999
15. Sutton MA, Ide J, Masters SE, et al. (2002) Interaction between amount and pattern of training in the induction of intermediate- and long-term memory for sensitization in Aplysia. *Learn Mem* 9: 29–40. https://doi.org/10.1101/lm.44802
16. Wainwright ML, Byrne JH, Cleary LJ (2004) Dissociation of morphological and physiological changes associated with long-term memory in Aplysia. *J Neurophysiol* 92: 2628–2632. https://doi.org/10.1152/jn.00335.2004
17. Wainwright ML, Zhang H, Byrne JH, et al. (2002) Localized neuronal outgrowth induced by long-term sensitization training in Aplysia. *J Neurosci* 22: 4132–4141. https://doi.org/10.1523/JNEUROSCI.22-10-04132.2002
18. Pettigrew D, Smolen P, Baxter DA, et al. (2005) Dynamic properties of regulatory motifs associated with induction of three temporal domains of memory in Aplysia. *J Comput Neurosci* 18: 163–181. https://doi.org/10.1007/s10827-005-6557-0
19. Song H, Smolen P, Av-Ron E, et al. (2006) Bifurcation and singularity analysis of a molecular network for the induction of long-term memory. *Biophys J* 90: 2309–2325 https://doi.org/10.1529/biophysj.105.074500
20. Dhooge A, Govearts W, Kuznetsov AY (2003) MATCONT: A MATLAB package for numerical bifurcation analysis of ODEs. *ACM T Math Software* 29: 141–164. https://doi.org/10.1145/779359.779362
21. Dhooge A, Govaerts W, Kuznetsov YA, et al. (2003) CL_MATCONT: A continuation toolbox in Matlab. *Proceedings of the 2003 ACM Symposium on Applied Computing* 161–166. https://doi.org/10.1145/952532.952567
22. KuznetsovYA (1998) *Elements of Applied Bifurcation Theory*, New York: Springer.
23. KuznetsovYA (2009) *Five Lectures on Numerical Bifurcation Analysis*, Utrecht University NL.
24. Govaerts WJF (2000) *Numerical Methods for Bifurcations of Dynamical Equilibria*, Society for Industrial and Applied Mathematics.
25. Flores-Tlacuahuac A, Morales P, Riveral-Toledo M. Multiobjective nonlinear model predictive control of a class of chemical reactors. *Ind Eng Chem Res* 51: 5891–5899. https://doi.org/10.1021/ie201742e
26. Sridhar LN (2021) Single and multiobjective optimal control of epidemic models involving vaccination and treatment. *J Biostat Epidemiol* 7: 25–35. https://doi.org/10.18502/jbe.v7i1.6292
27. Sridhar LN (2023) Bifurcation analysis and optimal control of the Crowley Martin phytoplankton-zooplankton model that considers the impact of nanoparticles. *Explo Mater Sci Res* 5: 54–60. https://dx.doi.org/10.47204/EMSR.5.1.2023.054-060
28. Sridhar LN (2020) Multiobjective nonlinear model predictive control of pharmaceutical batch crystallizers. *Drug Dev Ind Pharm* 46: 2089–2097. https://doi.org/10.1080/03639045.2020.1847135

29. Sridhar LN (2019) Multiobjective optimization and nonlinear model predictive control of the continuous fermentation process involving Saccharomyces Cerevisiae. *Biofuels* 13: 249–264. https://doi.org/10.1080/17597269.2019.1674000
30. Sridhar LN (2022) Single and multiobjective optimal control of the wastewater treatment process. *Trans Indian Natl Acad Eng* 7: 1339–1346. https://doi.org/10.1007/s41403-022-00368-6
31. Younis A, Dong Z (2023) Adaptive surrogate assisted multi-objective optimization approach for highly nonlinear and complex engineering design problems. *Appl Soft Comput* 150: 111065. https://doi.org/10.1016/j.asoc.2023.111065
32. Younis A, Dong Z (2022) High-fidelity surrogate based multi-objective optimization algorithm. *Algorithms* 15: 279. https://doi.org/10.3390/a15080279
33. Younis A, Dong Z (2010) Trends, features, and tests of common and recently introduced global optimization methods. *Eng Optimiz* 42: 691–718. https://doi.org/10.1080/03052150903386674
34. Safari A, Younis A, Wang G, et al. (2015) Development of a metamodel-assisted sampling approach to aerodynamic shape optimization problems. *J Mech Sci Technol* 29: 2013–2024. https://doi.org/10.1007/s12206-015-0422-5
35. Miettinen K (1999) *Nonlinear Multiobjective Optimization*, Berlin: Springer Science & Business Media.
36. Hart WE, Laird CD, Watson JP, et al. (2017) *Pyomo–Optimization Modeling in Python*, 2 Eds., Berlin: Springer.
37. Biegler LT (2007) An overview of simultaneous strategies for dynamic optimization. *Chem Eng Process* 46: 1043–1053. https://doi.org/10.1016/j.cep.2006.06.021
38. Wächter A, Biegler L (2006) On the implementation of an interior-point filter line-search algorithm for large-scale nonlinear programming. *Math Program* 106: 25–57. https://doi.org/10.1007/s10107-004-0559-y
39. Tawarmalani M, Sahinidis NV (2005) A polyhedral branch-and-cut approach to global optimization. *Math Program* 103: 225–249. https://doi.org/10.1007/s10107-005-0581-8

AIMS Press